

# Magnetically induced ring-current strengths of planar and nonplanar molecules: New insights from the pseudo- $\pi$ model

Mesías Orozco-Ic,<sup>1</sup> Maria Dimitrova,<sup>2</sup> Jorge Barroso,<sup>1</sup> Dage Sundholm,<sup>2,\*</sup> and Gabriel Merino.<sup>1,\*</sup>

<sup>1</sup>*Departamento de Física Aplicada, Centro de Investigación y de Estudios Avanzados, Unidad Mérida. Km 6 Antigua Carretera a Progreso. Apdo. Postal 73, Cordemex, 97310, Mérida, Yuc., México.*

<sup>2</sup>*Department of Chemistry, Faculty of Science, University of Helsinki, P.O. Box 55, A. I. Virtasen aukio 1, FIN-00014 Helsinki, Finland.*

## Abstract

The  $\pi$ -contribution to the magnetically induced current densities, ring-current strengths, and induced magnetic fields of large planar molecules (as kekulene) and three-dimensional molecules (as [10]cyclophenacene and chiral toroidal nanotubes C<sub>2016</sub> and C<sub>2196</sub>) have been computed using the pseudo- $\pi$  model with the gauge-including magnetically induced currents method. The magnetic response analysis shows that  $\pi$ -electrons are the main actors of the electron delocalization in carbon systems regardless of their size, suggesting that the  $\pi$ -component of the ring-current strengths can be used for assessing the aromatic character of this kind of molecules. Computations using the pseudo- $\pi$  model yield current densities and induced magnetic fields that are not contaminated by contributions from core and  $\sigma$ -electrons allowing investigations of large molecular structures as polycyclic aromatic hydrocarbons and cylindrical or toroidal carbon nanotubes.

## Introduction

In the presence of an external magnetic field, the interaction between the angular momentum of the electrons and a magnetic field produces an induced current density and concomitantly an induced magnetic field.<sup>1-3</sup> For molecules classified as aromatic, the magnetic response is mostly diamagnetic and is associated with a diatropic ring current around the ring.<sup>4</sup> In contrast, antiaromatic molecules sustain a net paratropic ring current that may lead to paramagnetism.<sup>5</sup> Several tools are now available to study the magnetic response of molecules;<sup>6-9</sup> however, for large systems, such analysis is computationally expensive and almost unviable.

In organic systems, it is well-accepted that the  $\pi$ -cloud is responsible for aromaticity.<sup>10,11</sup> One way to quantify this degree of delocalization is via the ring-current strength, which results from integrating the current density flowing through a given plane.<sup>12</sup> However, standard ring-current strength computations provide an all-electron magnetic response, and splitting it into its orbital components (core +  $\sigma$  +  $\pi$ ) is relatively expensive and practically unexplored for large systems. In 2002, Fowler and Steiner proposed an elegant approach, called the pseudo- $\pi$  model, to compute the  $\pi$ -component of the magnetically induced current densities.<sup>13</sup> It takes advantage of the symmetry of the out-of-plane  $\pi$ -orbitals in carbon molecules. The  $\pi$ -orbitals are represented by  $\sigma$ -orbitals constructed by removing all hydrogens and replacing carbons with hydrogen atoms. These hypothetical systems accurately mimic the ring current of the  $\pi$ -electrons, drastically reducing the computational cost. Interestingly, the main features of the induced magnetic field can also be reproduced by the pseudo- $\pi$  model.<sup>14</sup> So, the pseudo- $\pi$  model offers a cheap and straightforward way to estimate the  $\pi$ -component of the ring-current strengths and the induced magnetic field in large carbon structures.

Herein, we evaluate the  $\pi$ -component of the magnetically induced current densities, the ring-current strengths, and the induced magnetic field using the pseudo- $\pi$  model in a series of planar and non-planar molecules. Our set of molecules includes benzene as a reference for aromatic systems; naphthalene, anthracene, coronene, and kekulene as examples to understand the magnetic consequences of fused rings; cyclobutadiene, represent the antiaromatic case; C<sub>60</sub> and guadiene C<sub>72</sub> are examples of spherical clusters; [7]helicene and [10]cyclophenacene have helical and cylindrical topologies, respectively, and finally, the toroids C<sub>2016</sub> and C<sub>2196</sub> are the icing on the cake.

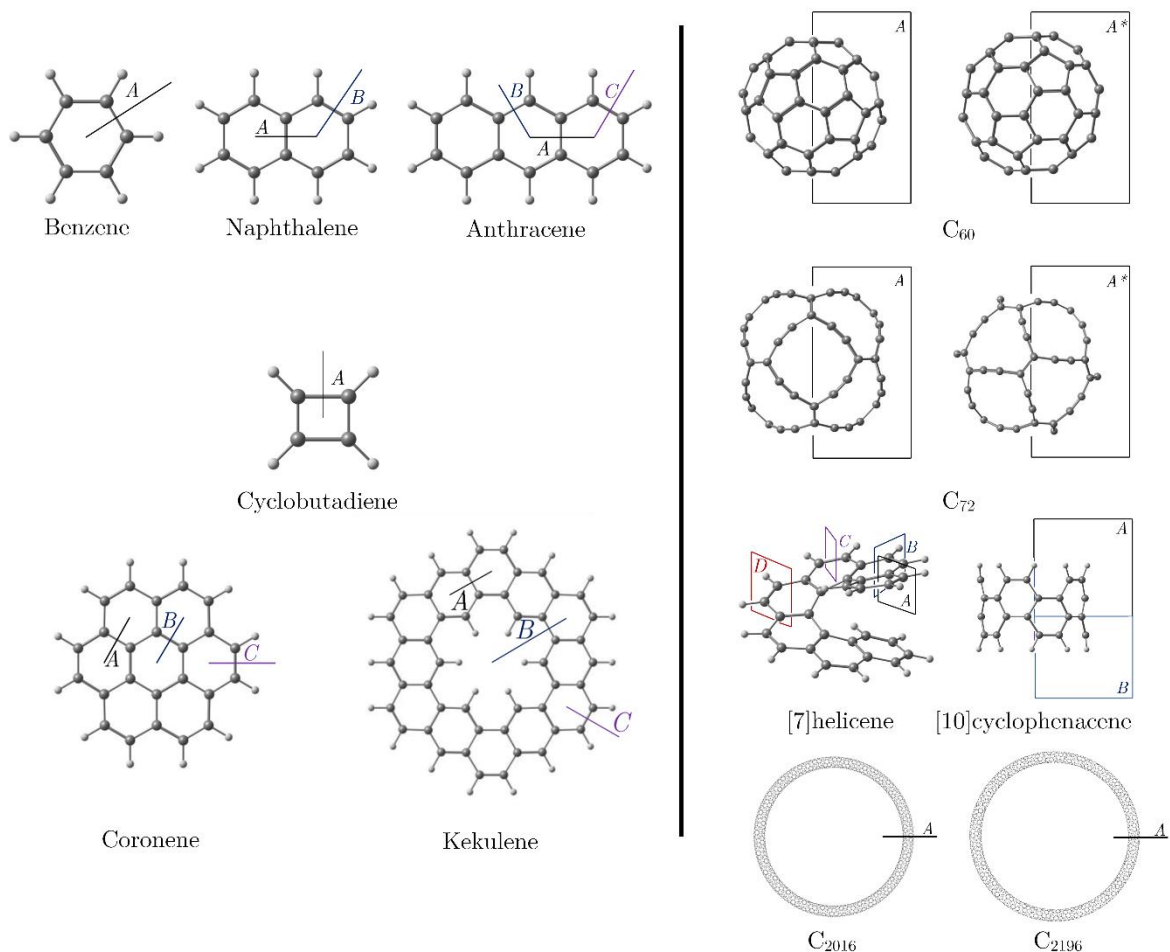


**Figure 1.** The studied planar (left) and non-planar (right) molecules. The integration planes are extended 8 bohr above and below the molecular planes in planar structures,  $C_{60}$  and guadiene ( $C_{72}$ ), 4 bohr for helicene, 6 bohr for [10]cyclophenacene (measured from hydrogens molecular plane), and 11 bohr for toroidal  $C_{2016}$  and  $C_{2196}$ .

## Computational Details

Since geometries of the organic molecules are well-described by the B3LYP<sup>15</sup> functional and it also provides ring-current strengths that agree with those computed at the MP2 level or at CCSD(T) levels,<sup>5,16-18</sup> all geometries were fully optimized using the B3LYP approach in conjunction with a Grimme's D3(BJ) dispersion correction<sup>19</sup> and a def2-TZVP basis set.<sup>20</sup> Nuclear magnetic resonance computations were carried out at the B3LYP/def2-TZVP level using gauge-including atomic orbitals (GIAOs).<sup>21,22</sup> For  $C_{2016}$  and  $C_{2196}$ , the def2-SVP basis set<sup>20</sup> was selected. All computations were performed with the Turbomole program.<sup>23,24</sup> The susceptibility of the magnetically induced current density<sup>8,12,25</sup> ( $\mathbf{J}^{\text{ind}}$ ) and the first derivative of the induced magnetic field<sup>9,26,27</sup> ( $\mathbf{B}^{\text{ind}}$ ) with respect to the external magnetic

field were computed in the zero-field limit ( $\mathbf{B}^{\text{ext}} \rightarrow 0$ ). Thus,  $\mathbf{J}^{\text{ind}}$  and  $\mathbf{B}^{\text{ind}}$  are linearly dependent on the strength of the external magnetic field.  $\mathbf{J}^{\text{ind}}$  and  $\mathbf{B}^{\text{ind}}$  computations were performed using the GIMIC<sup>8,12,25</sup> and Aromagnetic<sup>28</sup> programs, respectively. The external magnetic field was applied parallel to the molecular axis of the highest-symmetry ( $z$ -axis) to induce the maximum ring currents and secondary magnetic fields.<sup>29</sup> In this orientation, the most significant vector contribution to  $\mathbf{B}^{\text{ind}}$  comes from the  $z$ -component ( $B^{\text{ind}}_z$ ). This scalar field is equal to the  $zz$ -component of the nucleus-independent chemical shifts (NICS<sub>zz</sub>) in planar molecules.<sup>6,30</sup> Ring-current strengths are obtained by integrating the current density  $\mathbf{J}^{\text{ind}}$  in a plane perpendicular to the molecular ring, intersecting a specific bond or the entire molecular ring.<sup>8,12,25</sup> The integration planes are illustrated in Figure 1. The total  $\mathbf{J}^{\text{ind}}$  and  $\mathbf{B}^{\text{ind}}$  are obtained by performing all-electron computations on the original carbon-based molecules. In contrast, the pseudo- $\pi$  contributions to  $\mathbf{J}^{\text{ind}}$  and  $\mathbf{B}^{\text{ind}}$  are obtained by performing computations on molecular systems with all hydrogen atoms omitted, and hydrogen atoms replace carbon. Visual representations of  $\mathbf{J}^{\text{ind}}$  and  $\mathbf{B}^{\text{ind}}$  were created using Paraview<sup>31</sup> and VisIt<sup>32</sup>, respectively. The units for the ring-current strengths and  $B^{\text{ind}}_z$  are nA/T ppm, respectively.

## Benzene

Benzene is the aromatic system *par excellence*. The pseudo- $\pi$  computations of  $\mathbf{J}^{\text{ind}}$  ( ${}^{\text{p}\pi}\mathbf{J}^{\text{ind}}$ ) is entirely diatropic throughout the space (see Figure 2a), which explains why the magnetic response of  $\pi$ -electrons obey a classic ring-current pattern,<sup>33</sup> but more importantly,  ${}^{\text{p}\pi}\mathbf{J}^{\text{ind}}$  successfully reproduces the global pattern of the true  $\pi$ -component of  $\mathbf{J}^{\text{ind}}$ . Fowler and Steiner showed that the maximum value of the in-plane  ${}^{\text{p}\pi}\mathbf{J}^{\text{ind}}$  is 0.0788 a.u., in agreement with the maximum of 0.0790 a.u. in true  $\pi$ -current computed using the ipsocentric method.<sup>13</sup>

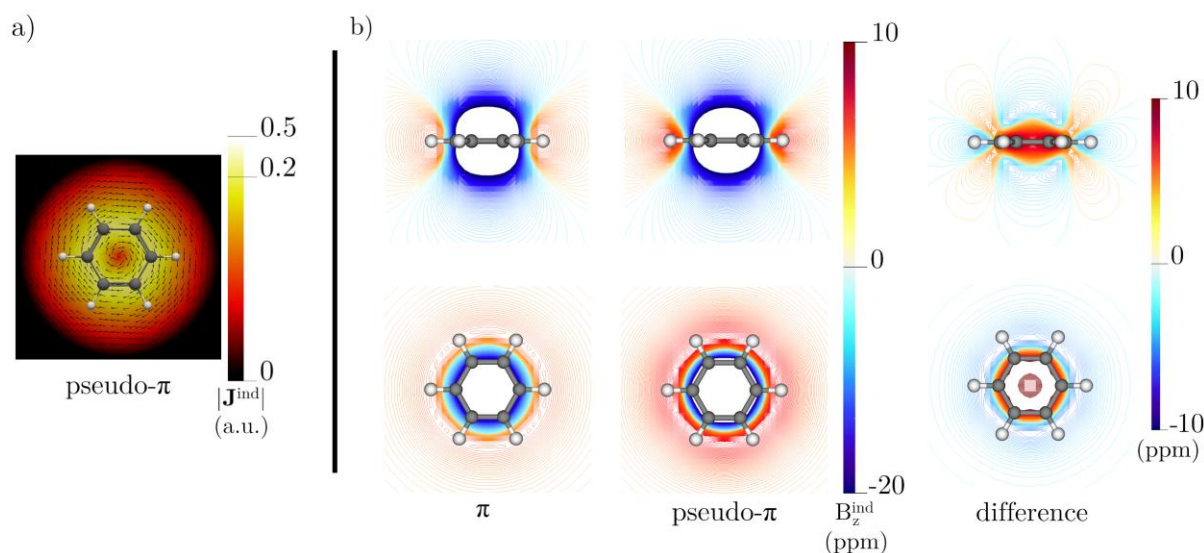


**Figure 2.** a) The  ${}^{\text{p}\pi}\mathbf{J}^{\text{ind}}$  calculated in the molecular plane of benzene. The arrows indicate the direction of the current density. The  $|\mathbf{J}^{\text{ind}}|$  scale is given in atomic units (1 a.u. = 100.63 nA/T/Å<sup>2</sup>). b) Comparison of the true  $\pi$ -component of  $B_z^{\text{ind}}$  (left), the pseudo- $\pi$  modeled (in the middle), and the difference resulting from subtracting the pseudo- $\pi$  component from the true  $\pi$ -component computed in the same grid (right) for benzene. The enclosed white areas delimiting the shielding (or deshielding) cones correspond to regions that are more negative (or more positive) on the corresponding scale.

Charistos *et al.*<sup>14</sup> showed that the pseudo- $\pi$  model also mimics the  $\pi$ -component for  $\mathbf{B}^{\text{ind}}$  ( ${}^{\text{p}\pi}\mathbf{B}^{\text{ind}}$ ). They noted that the value of  $B_z^{\text{ind}}$  computed using the pseudo- $\pi$  approach ( ${}^{\text{p}\pi}B_z^{\text{ind}}$ ) at the ring center deviates of barely 10% from that of the true  $\pi$ -component and this difference decreases for long distances along the  $z$ -axis. The authors remarked that variations in size and shape are negligible and there is a slight overestimation of the  $\pi$ -magnetic response near the plane of the ring.

Let us compare the true  $\pi$ -contribution of  $B_z^{\text{ind}}$  and  ${}^{\text{p}\pi}B_z^{\text{ind}}$  to determine whether the model mimics the  $\pi$ -electrons in the whole space and its accuracy. Figure 2b shows the difference between the two scalar fields red/blue regions indicating the  ${}^{\text{p}\pi}B_z^{\text{ind}}$  values are over/underestimated. The most noticeable overestimated values are found near the ring center and the carbon skeleton, but also and the boundary region of the shielding cone. In contrast, the shielding cone is reasonably well-described with a small underestimation.

What else could we extract from the pseudo- $\pi$  model to diagnose electron delocalization? As mentioned, one way to quantify this degree of delocalization is through the ring-current strength. Previous current-density computations yield a ring-current strength of 12.0 nA/T.<sup>8,12,25</sup> including the core-,  $\sigma$ -, and  $\pi$ -electrons contributions. Table 1 summarizes the total ring-current strengths and those computed using  ${}^{\text{p}\pi}\mathbf{J}^{\text{ind}}$ , separated into their diatropic and

paratropic terms. The ring-current strength obtained from  ${}^{p\pi}\mathbf{J}^{\text{ind}}$  is purely diatropic (12.4 nA/T). This number is in excellent agreement with that reported by Monaco et al. (11.7 nA/T at HF level) for the true  $\pi$ -contribution.<sup>34</sup> So, the pseudo- $\pi$  model is suitable for providing snapshots of the ring current and induced magnetic field and giving precise numbers such as the ring-current strength.

**Table 1.** Diatropic and paratropic contributions to the net ring-current strength (in nA/T) for the planar molecules computed at the B3LYP/def2-TZVP level. The position of the integration planes is shown in Figure 1.

Molecule	Plane	total			pseudo- $\pi$		
		diatropic	paratropic	net	diatropic	paratropic	net
Benzene	A	16.99	-4.94	12.05	12.42	0.00	12.42
Cyclobutadiene	A	2.66	-22.54	-19.88	0.00	-27.04	-27.04
Naphthalene	A	7.72	-7.72	0.00	0.41	-0.41	0.00
	B	17.83	-4.75	13.08	13.41	0.00	13.41
Anthracene	A	9.77	-6.13	3.64	3.62	-0.06	3.56
	B	19.02	-4.20	15.70	16.36	0.00	16.36
	C	17.08	-4.79	12.28	12.86	0.00	12.86
Coronene	A	7.60	-7.60	0.00	0.25	-0.25	0.00
	B	6.06	-11.38	-5.32	0.00	-5.18	-5.18
	C	21.53	-4.02	17.51	18.41	0.00	18.41
Kekulene	A	10.88	-5.96	4.91	4.50	0.00	4.50
	B	5.87	-14.13	-8.26	1.01	-8.77	-7.76
	C	15.39	-5.30	10.09	11.29	0.00	11.29

## Cyclobutadiene

The second obvious system to analyze is cyclobutadiene, the quintessential case of antiaromaticity. For this molecule, there is no reference for the true  $\pi$ -component of the ring-current, so we limit ourselves to describing the variations between the  $\pi$ -component of  $B_z^{\text{ind}}$  values and those obtained by  ${}^{\text{p}\pi}B_z^{\text{ind}}$  (see Figure 3a). Note that the shape of the deshielding cone of both scalar fields is similar. However,  ${}^{\text{p}\pi}B_z^{\text{ind}}$  significantly overestimated the deshielding values near the molecular plane, in particular, it exaggerates the absolute values at the ring center by almost a factor of two.<sup>14</sup> This leads to notable negative differences above (and below) the ring. So, the pseudo- $\pi$  model response in this antiaromatic system is qualitatively enough to provide a diagnosis of antiaromaticity, but a quantitative interpretation is not reliable.

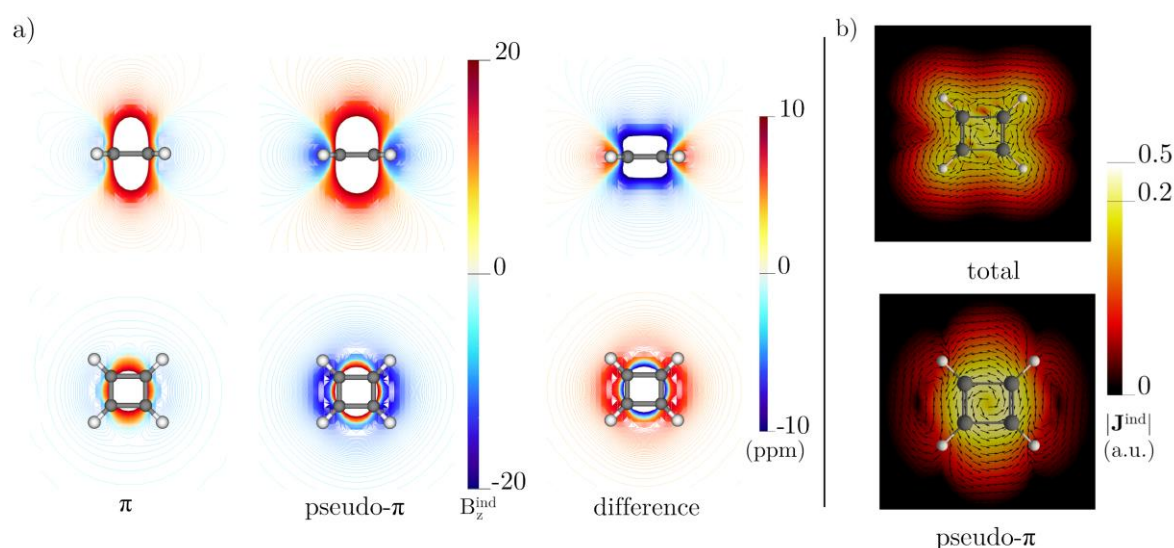


**Figure 3.** a) Comparison of the true  $\pi$ -component of  $B_z^{\text{ind}}$  (left), the pseudo- $\pi$  modeled (in the middle), and the difference resulting from subtracting the pseudo- $\pi$  component from the true  $\pi$ -component computed in the same grid (right) for cyclobutadiene. b) The total  $\mathbf{J}^{\text{ind}}$  (top) and  ${}^{\text{p}\pi}\mathbf{J}^{\text{ind}}$  (bottom) calculated in the molecular plane of cyclobutadiene. The arrows indicate the direction of the current density. The  $|\mathbf{J}^{\text{ind}}|$  scale is given in atomic units (1 a.u. = 100.63 nA/T/Å<sup>2</sup>).

If the deshielding values are overestimated, then  ${}^{\text{p}\pi}\mathbf{J}^{\text{ind}}$  are also amplified, although qualitatively correct in their diagnosis. The total  $\mathbf{J}^{\text{ind}}$  indicates that the current is paratropic inside the ring and diatropic on outside (Figure 3b). The same is true for  ${}^{\text{p}\pi}\mathbf{J}^{\text{ind}}$ , where there is also a counterclockwise ring current flowing both inside and outside the ring. Besides,  ${}^{\text{p}\pi}\mathbf{J}^{\text{ind}}$  provides large positive  $|\mathbf{J}^{\text{ind}}|$  values along the perimeter, leading to a strong paratropic ring

current strength for cyclobutadiene (-27.04 nA/T, see Table 1). Although the overestimation of the magnetic response by the pseudo- $\pi$  model can be a limiting factor for the study of antiaromatic molecules,<sup>13,14</sup> qualitatively the magnetic behavior is correct and can be used as a first approximation for the description of antiaromaticity. The model gives rather accurate ring-current strengths for aromatic molecules but overestimates them and the  $B_z^{\text{ind}}$  values for antiaromatic molecules.<sup>13,14</sup> Notice that antiaromaticity and its prototypical paramagnetic response has been discussed as being intimately related to the symmetry of the system.<sup>35</sup> Additionally, the ring-current strengths of strongly antiaromatic molecules tend to be overestimated when functionals with none or little Hartree-Fock exchange are employed. A better agreement, with values obtained at the MP2 level, is achieved when the functional includes at least 50% of Hartree-Fock exchange.<sup>17,18,36-38</sup>

### Naphthalene and anthracene

For naphthalene, the magnitude and shape of  ${}^{\text{p}\pi}\mathbf{B}_z^{\text{ind}}$  are quite similar to those of the  $\pi$ -component for  $\mathbf{B}^{\text{ind}}$ . Only slight differences are perceived near the molecular plane (see Figure S1).  ${}^{\text{p}\pi}\mathbf{J}^{\text{ind}}$  reveals a ring current pathway around the perimeter of the molecule, very similar to that provided by the  $\pi$ -electrons.<sup>39,40</sup> In that case, the paratropic ring currents determined by the total  $\mathbf{J}^{\text{ind}}$  inside the rings originate from the  $\sigma$ -electrons (see Figure S2).<sup>39,40</sup> The positive and negative contributions to the pseudo- $\pi$  current density in the C4a-C8a bond are practically negligible ( $\pm 0.41$  nA/T). In contrast, the positive and negative components are  $\pm 7.72$  nA/T for the total  $\mathbf{J}^{\text{ind}}$ , which also implies a considerable current density flow in the shared C-C bond due to the  $\sigma$ -electrons.

As Charistos *et al.* argued, the  ${}^{\text{p}\pi}\mathbf{B}_z^{\text{ind}}$  computations reproduce the shape and values of the true  $\pi$ -component.<sup>14</sup> For naphthalene, both rings produce a similar size of shielding cone, whereas for anthracene, the central ring cone is more prominent in magnitude and size, with larger negative values at the central ring. However, this scalar field gives no information about local or peripheral current pathways (see Figure S2).  ${}^{\text{p}\pi}\mathbf{J}^{\text{ind}}$  of anthracene is diatropic inside and outside the carbon skeleton with a localized ring current in the central ring (see Figure S3). The true  $\pi$ -component of  $\mathbf{J}^{\text{ind}}$  is practically identical to  ${}^{\text{p}\pi}\mathbf{J}^{\text{ind}}$ .<sup>39,40</sup> The integrated ring-current strengths from  ${}^{\text{p}\pi}\mathbf{J}^{\text{ind}}$  give rise local ring-current strength of 3.56 nA/T in the inner ring and a peripheral pseudo- $\pi$  ring-current of 12.90 nA/T, which is almost the same as for benzene. Thus, the ring current of anthracene is slightly weaker than that of naphthalene, even though anthracene has more  $\pi$ -electrons.

## Coronene and kekulene

Coronene is another interesting polycyclic aromatic hydrocarbon (PAH) that exhibits two concentric ring currents flowing in opposite directions.<sup>41,42</sup> Since the  $\pi$ -response in polycyclic systems is correctly emulated by the pseudo- $\pi$  model,<sup>13,14,43</sup> we will hereafter assume the  $\pi$ -component as the one predicted by such approach. The  ${}^{p\pi}B_z^{\text{ind}}$  calculations show a shielded response, which in the molecular plane has negative values even in the inner hub. Thus, although the  $\pi$ -component of the shielding provides better correlation with the ring currents,  ${}^{p\pi}B_z^{\text{ind}}$  (and also NICS) cannot identify the existence of the paratropic ring current of the hub (Figure 4).

In contrast,  ${}^{p\pi}J^{\text{ind}}$  indicates a paratropic ring current in the inner hub (the innermost ring), while the ring current along the outer edge is diatropic (Figure 4).  ${}^{p\pi}J^{\text{ind}}$  produces a diatropic peripheral ring current and an inner paratropic one in the central ring. In other words, the paratropic flux (of -5.18 nA/T) due to the strong diatropic pseudo- $\pi$  current (18.41 nA/T) flowing around the coronene rim promotes a shielding cone that suppresses the deshielding induced by the paratropic ring current of the inner hub. This is the reason why  ${}^{p\pi}B_z^{\text{ind}}$  does not exhibit deshielded values in that ring. The ring-current strengths for the paratropic and diatropic currents for the total calculation (-5.32 and 17.51 nA/T, respectively) are similar to those of  ${}^{p\pi}J^{\text{ind}}$  (see Table 1). Compared to the total responses, the paratropic ring-current strength and the  ${}^{p\pi}B_z^{\text{ind}}$  values of the hub are not overestimated as for cyclobutadiene. This probably occurs because the inner central ring of the coronene is highly symmetrical.

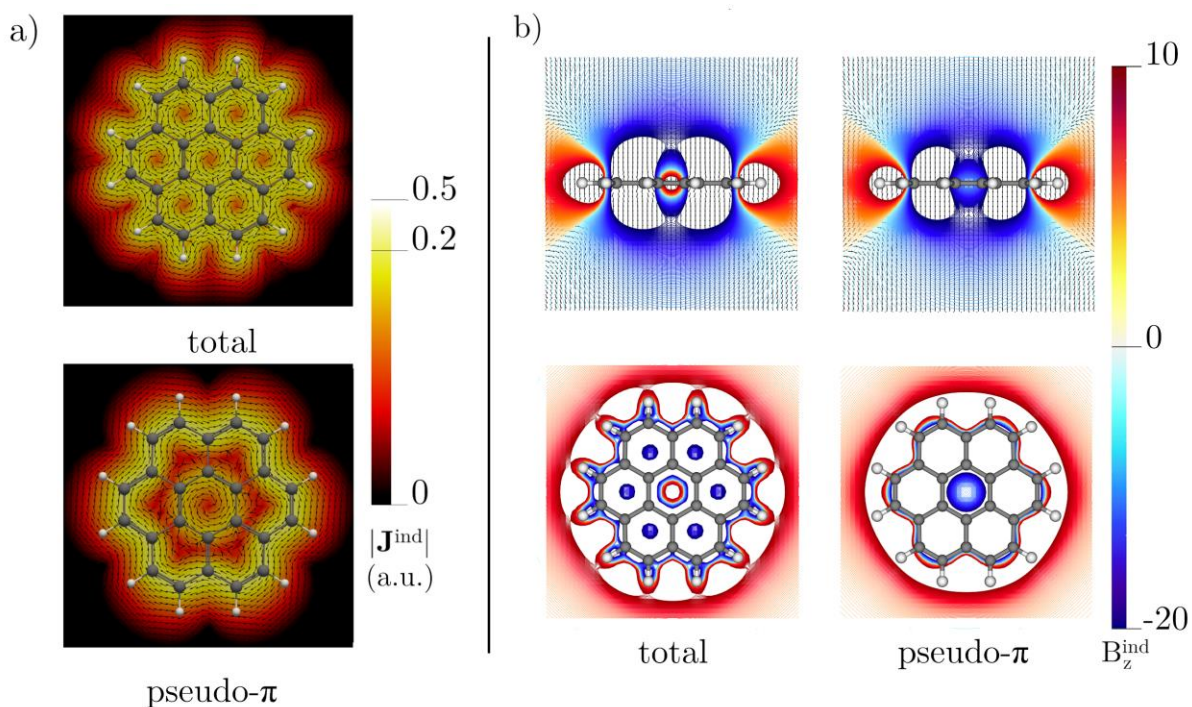


**Figure 4.** a) The total  $\mathbf{J}^{\text{ind}}$  (top) and  ${}^{\text{p}\pi}\mathbf{J}^{\text{ind}}$  (bottom) calculated in the molecular plane of coronene. The arrows indicate the direction of the current density. The  $|\mathbf{J}^{\text{ind}}|$  scale is given in atomic units (1 a.u. = 100.63 nA/T/Å<sup>2</sup>). b) The total  $\mathbf{B}^{\text{ind}}$  (left) and the  ${}^{\text{p}\pi}\mathbf{B}^{\text{ind}}$  (right) calculated in the transverse plane (top) and in the molecular plane (bottom) of coronene. The arrows show the direction of  $\mathbf{B}^{\text{ind}}$ , while the color scale denotes the strength of  $B_z^{\text{ind}}$ .

Kekulene has been pointed out as superomatic.<sup>44,45</sup> Like coronene, kekulene exhibits counter-rotating currents.<sup>46</sup> For systems of such size, the model becomes quite convenient because a true  $\pi$ -component computation is very demanding on computational resources.  ${}^{\text{p}\pi}\mathbf{J}^{\text{ind}}$  in kekulene yields a fully diatropic ring current of 11.29 nA/T along the outer edge and a paratropic current of -7.76 nA/T inside the inner kekulene contour. The six-membered rings (6-MRs) between the corners of kekulene have an additional local pseudo- $\pi$  ring current (similar to that of anthracene) of 4.50 nA/T. These rings have more equidistant C-C bonds than the corner rings. The total ring-current strengths do not differ significantly from those obtained with  ${}^{\text{p}\pi}\mathbf{J}^{\text{ind}}$ , revealing that  $\pi$ -electrons are responsible for the counter-rotating currents (Figure 5). The peripheral ring current is weaker than that of coronene, giving rise to a shielding cone that does not entirely suppress the deshielding cone induced by the inner paratropic current, leading to negative  ${}^{\text{p}\pi}B_z^{\text{ind}}$  values at the center of kekulene. The local ring currents lead to differences in the shielding inside the 6-MRs (Figure 5). Specifically, the  ${}^{\text{p}\pi}B_z^{\text{ind}}$  values are more negative in the 6-MRs between the corners than at the corners, resulting from the local  $\pi$ -

circulations. These rings even exhibit positive  $B_z^{\text{ind}}$  values inside the ring. Finally, the ring-current strength, calculated in a plane from the center of the molecule outwards intersecting both current pathways, is weakly diatropic with a total ring-current strength of 1.83 nA/T, which is half the value obtained with the pseudo- $\pi$  model. In general, none of the values found for the ring-current strengths or shielding can be associated with a superaromatic character. Moreover, for the inner hub of kekulene,  ${}^{p\pi}\mathbf{J}^{\text{ind}}$  and  ${}^{p\pi}B_z^{\text{ind}}$  do not seem to be overestimated. The paratropic current can be considered as a superposition of the magnetic response of the individual rings and, like coronene, the inner contour is symmetric.

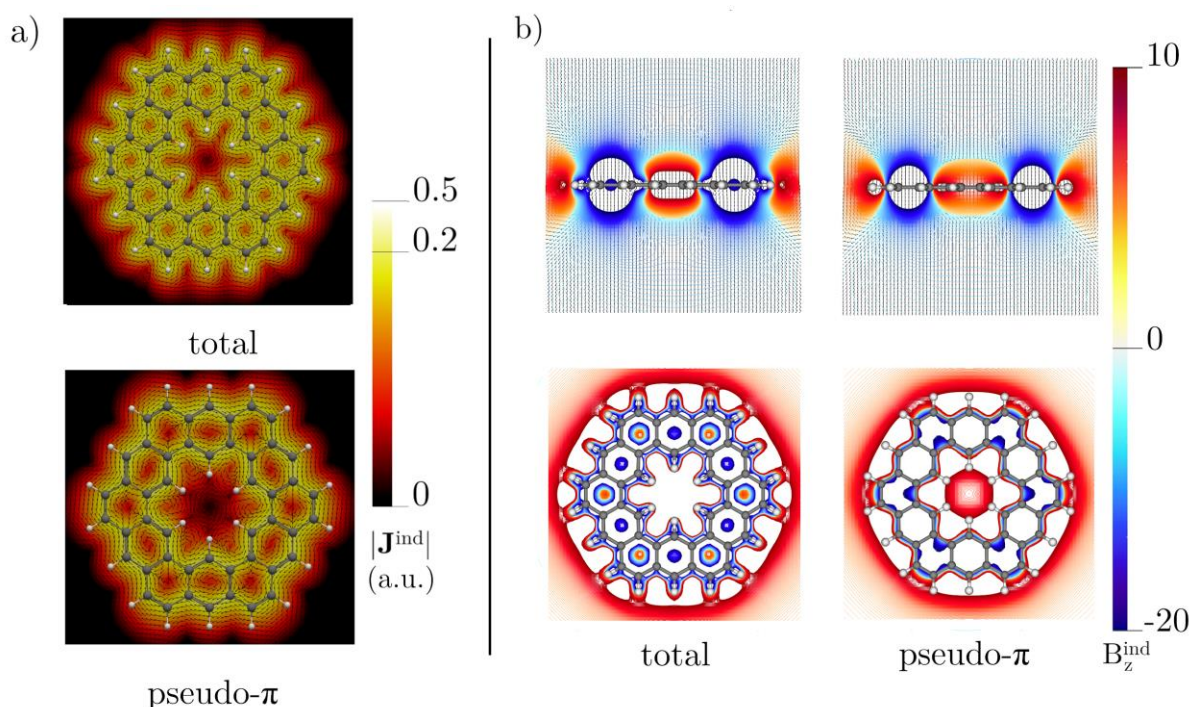


**Figure 5.** a) The total  $\mathbf{J}^{\text{ind}}$  (top) and  ${}^{p\pi}\mathbf{J}^{\text{ind}}$  (bottom) calculated in the molecular plane of kekulene. The arrows indicate the direction of the current density. The  $|\mathbf{J}^{\text{ind}}|$  scale is given in atomic units (1 a.u. = 100.63 nA/T/Å<sup>2</sup>). b) The total  $\mathbf{B}^{\text{ind}}$  (left) and the  ${}^{p\pi}\mathbf{B}^{\text{ind}}$  (right) calculated in the transverse plane (top) and in the molecular plane (bottom) of kekulene. The arrows show the direction of  $\mathbf{B}^{\text{ind}}$ , while the color scale denotes the strength of  $B_z^{\text{ind}}$ .

### Fullerene and guadiene

From a magnetic point of view, C<sub>60</sub> has been classified as non-aromatic.<sup>47-50</sup> The  $B_z^{\text{ind}}$  plots of C<sub>60</sub> exhibit several local shielded and deshielded regions (Figure 6a), which could lead to different responses depending on the orientation of the external field.  ${}^{p\pi}B_z^{\text{ind}}$  shows that the inside of the cage is deshielded due to an inner paratropic current.  ${}^{p\pi}\mathbf{J}^{\text{ind}}$  reveals that the 6-MRs form a spherical pathway around the entire molecule (see Figure 6b). However, the five-

membered rings (5-MRs) exhibit a somewhat overestimated dehielings. In addition, the spherical current is distorted due to the local paratropic ring currents in the 5-MRs. Previous reports of the total  $\mathbf{J}^{\text{ind}}$  indicate a weak diatropic ring current when the magnetic field is applied parallel to a  $C_3$  axis, but when the magnetic field is applied parallel to a  $C_5$  axis, a paratropic ring current predominates. Besides, the spherical-like ring currents inside and outside the carbon skeleton flow in opposite directions, paratropically and diatropically, respectively.<sup>49</sup> Compared to the total,  ${}^{\text{p}\pi}\mathbf{J}^{\text{ind}}$  provides a clearer picture of the paratropic and diatropic fluxes. Table 2 lists the global ring-current strengths of  $C_{60}$  calculated with the external field perpendicularly to the six- (plane A) and 5-MRs (plane A\*), respectively. The net pseudo- $\pi$  current strength is weakly (-1.76 nA/T) and strongly paratropic (-25.91 nA/T) when the magnetic field is oriented parallel to the  $C_3$  and  $C_5$  axis, respectively, because the 5-MRs maintain very strong local paratropic ring currents.<sup>49</sup> So, strictly speaking,  $C_{60}$  is not spherically aromatic, regardless of the magnetic field orientation, the net pseudo- $\pi$  ring-current strength is paratropic conferring an antiaromatic character for  $C_{60}$ .

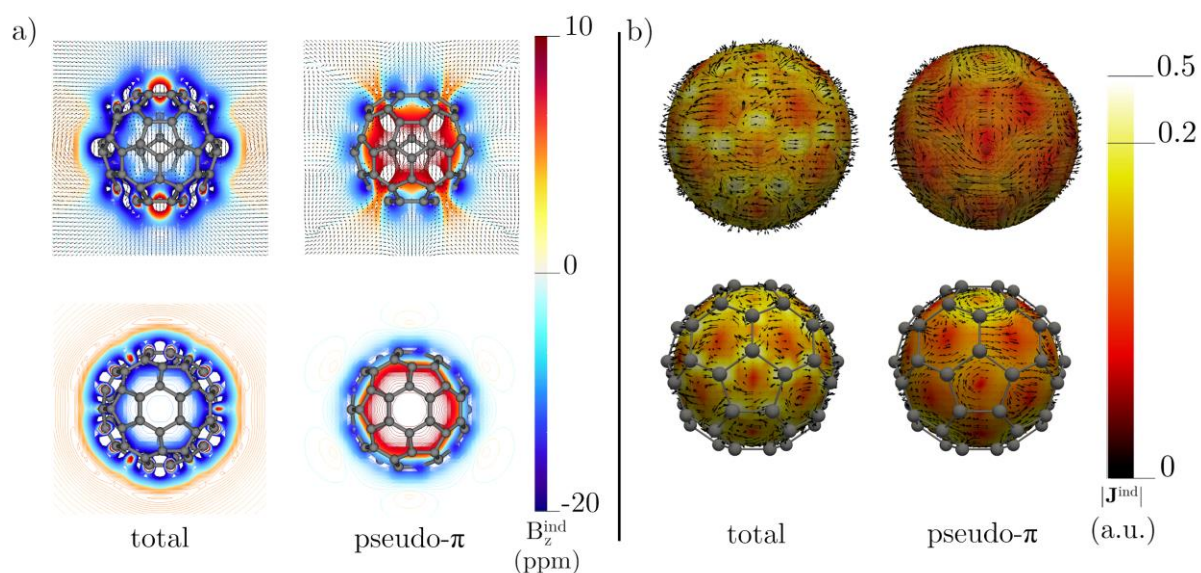


**Figure 6.** a) The total  $\mathbf{B}^{\text{ind}}$  (left) and the  ${}^{\text{p}\pi}\mathbf{B}^{\text{ind}}$  (right) calculated in a plane parallel (top) and a perpendicular plane ( $z = 0$ ) to the external field (bottom) for  $C_{60}$ . The arrows show the direction of  $\mathbf{B}^{\text{ind}}$ , while the color scale denotes the strength of  $B_z^{\text{ind}}$ . b) The total  $\mathbf{J}^{\text{ind}}$  (left) and  ${}^{\text{p}\pi}\mathbf{J}^{\text{ind}}$  (right) calculated 1 bohr outside (top) and 1 bohr inside (bottom) the molecular surface of fullerene ( $C_{60}$ ). The arrows show the direction of the current density. The  $|\mathbf{J}^{\text{ind}}|$  scale is given in atomic units (1 a.u. = 100.63 nA/T/Å<sup>2</sup>). The external field is parallel to the  $C_3$  axis.

**Table 2.** Diatropic and paratropic contributions to the net ring-current strength (in nA/T) for the nonplanar molecules computed at the B3LYP/def2-TZVP level. The position of the integration planes is shown in Figure 1.

Molecule	Plane	total			pseudo- $\pi$		
		diatropic	paratropic	net	diatropic	paratropic	net
C <sub>60</sub>	A	45.87	-44.48	1.39	15.65	-17.42	-1.76
	A*	37.15	-53.14	-15.99	9.00	-34.91	-25.91
C <sub>72</sub> (gaudiene)	A	56.96	-11.03	45.92	53.38	-0.34	53.04
	A*	51.32	-11.35	39.96	48.71	-0.60	48.10
[7]helicene	A	16.35	-4.26	12.09	13.25	-0.03	13.22
	B	15.61	-4.90	10.71	12.08	0.00	12.08
	C	15.76	-4.67	11.09	13.41	0.00	13.41
	D	16.58	-4.62	11.95	12.94	0.00	12.94
[10]cyclophenacene	A	2.24	-8.46	-6.22	0.09	-4.82	-4.73
	B	5.27	-7.28	-2.01	1.87	-3.71	-1.84
C <sub>2016</sub> (toroidal)	A	97.76 (314.28 <sup>†</sup> )	-60.05 (-21.96 <sup>†</sup> )	37.75 (292.30 <sup>†</sup> )	215.22 (417.90 <sup>†</sup> )	-4.79 (-1.23 <sup>†</sup> )	210.43 (416.65 <sup>†</sup> )
C <sub>2196</sub>	A	-	-	-	65.60 (314.32 <sup>†</sup> )	-5.90 (-0.36 <sup>†</sup> )	59.68 (313.96 <sup>†</sup> )

<sup>†</sup>Values computed at the TPSS/def2-SVP level.

Gaudiene (C<sub>72</sub>) can be graph-theoretically constructed by edge subdivisions and leapfrog transformations from cubic polyhedra or folding  $\beta$ -graphyne.<sup>51-53</sup> Next, the edges of eight hexadehydro[12]annulene rings form six four-sided rings (tetrahydro[12]annulenes) belonging to the  $O_h$  point group.<sup>51-53</sup> Gaudiene is expected to be spherically aromatic, according to Hirsch's rule<sup>54</sup> with  $n = 5$ . The holes are too large to allow a significant through-space current

density, which is a prerequisite for true spherical aromaticity.<sup>52,55</sup>  $\mathbf{J}^{\text{ind}}$  sustains strong global diatropic ring currents along the carbon bonds (Figure 7a). Although the total magnetic response of this cage has been reported,<sup>55</sup>  ${}^{\text{p}\pi}\mathbf{J}^{\text{ind}}$  reveals a similarity to the total. From this, it can be inferred that the large holes promote the  $\sigma$ -electrons not to distort the current-density topology considerably. The  ${}^{\text{p}\pi}\mathbf{J}^{\text{ind}}$  pathways inside and outside the cage lead to strong global ring currents of 53.04 and 48.10 nA/T when the magnetic field is perpendicular to the 6-MRs and four-membered rings (4-MRs), respectively (see Table 2). Then, gaudiene is an aromatic sphere that gives rise to a shielding cone similar to benzene (Figure 7b). The  ${}^{\text{p}\pi}\mathbf{B}_z^{\text{ind}}$  shielding cone is relatively uniform when the magnetic field is perpendicular to a 6-MR and perpendicular to the 4-MRs, respectively.

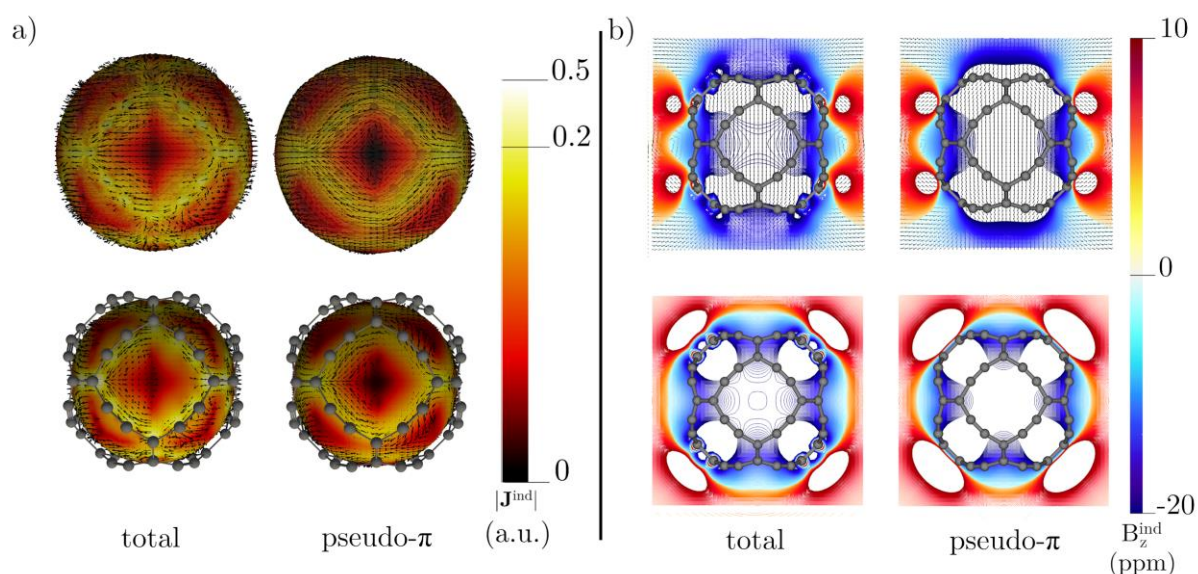


**Figure 7.** a) The total  $\mathbf{J}^{\text{ind}}$  (left) and  ${}^{\text{p}\pi}\mathbf{J}^{\text{ind}}$  (right) calculated 1 bohr outside (top) and 1 bohr inside (bottom) the molecular surface of gaudiene. The arrows show the direction of the current density. The  $|\mathbf{J}^{\text{ind}}|$  scale is given in atomic units (1 a.u. = 100.63 nA/T/Å<sup>2</sup>). b) The total  $\mathbf{B}^{\text{ind}}$  (left) and the  ${}^{\text{p}\pi}\mathbf{B}^{\text{ind}}$  (right) calculated in a plane parallel (top) and a perpendicular plane ( $z = 0$ ) to the external field (bottom) for gaudiene. The arrows show the direction of  $\mathbf{B}^{\text{ind}}$ , while the color scale denotes the strength of  $B_z^{\text{ind}}$ . The external field is perpendicular to a 4-MR.

### [7]helicene

[7]helicene consists of seven 6-MRs fused and twisted around the symmetry axis, forming a cylindrical helix. Since helicenes consist of several rings forming a nonplanar structure with conjugated bonds and delocalized  $\pi$ -electrons, evaluating their aromatic character based on studies of magnetic properties has led to different conclusions.<sup>56-60</sup> In the

case of the  $\mathbf{B}^{\text{ind}}$  analysis, the  $\pi$ -contribution to  $B_z^{\text{ind}}$  has a deshielded zone along the helical axis that grows with the number of rings in the helicene, giving rise to anomalous shieldings in the individual rings.<sup>56</sup> This behavior is reproduced by our  ${}^{\text{p}\pi}\mathbf{B}_z^{\text{ind}}$  computations. This deshielding cone is a direct consequence of a diatropic  ${}^{\text{p}\pi}\mathbf{J}^{\text{ind}}$  flowing along the periphery and back into the helical skeleton (see Figure 8). It is caused by the overlap of small external paramagnetic zones of each ring. The ring-current strengths in Table 2 are those corresponding to each ring. The terminal rings have stronger total ring currents, as Cherni *et al.* stated.<sup>57</sup> However,  ${}^{\text{p}\pi}\mathbf{J}^{\text{ind}}$  of the individual rings is diatropic with very similar ring-current strengths in the range of 12.08 - 13.41 nA/T, suggesting that all the 6-MRs have approximately the same degree of delocalization despite stacking. Therefore, the correct diagnosis of aromaticity via magnetic criteria must be carried out by considering the  $\pi$ -electrons contributions to the ring-current strengths.

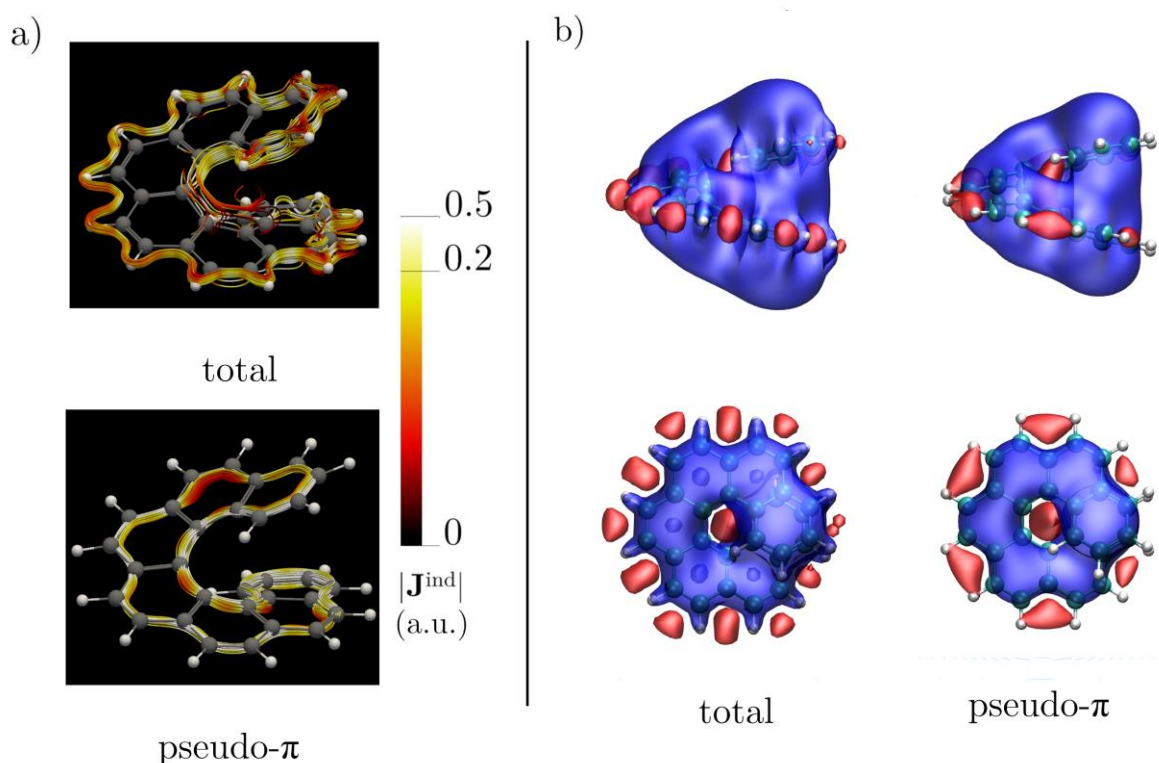


**Figure 8.** a) Streamlines representation of the total  $\mathbf{J}^{\text{ind}}$  (top) and  ${}^{\text{p}\pi}\mathbf{J}^{\text{ind}}$  (bottom) calculated in the molecular plane of [7]helicene. The arrows indicate the direction of the current density. The  $|\mathbf{J}^{\text{ind}}|$  scale is given in atomic units (1 a.u. = 100.63 nA/T/Å<sup>2</sup>). b) The isosurfaces of the total  $B_z^{\text{ind}}$  (left) and the  ${}^{\text{p}\pi}B_z^{\text{ind}}$  (right) of [7]helicene. The shielding (-10 ppm) and deshielding (10 ppm) cones are shown in blue and red, respectively. The external field is parallel to the helical axis.

## [10]cyclophenacene

[10]cyclophenacene is composed of 6-MRs zigzag fused to form a cylindrical belt.<sup>61-65</sup> This molecule is considered a predecessor of carbon nanotubes (CNT) and the evaluation of its magnetic response is challenging due to the presence of  $\pi$ -electrons wrapped in a cylinder.<sup>66-68</sup> Our  $^{p\pi}\mathbf{J}^{\text{ind}}$  computations reveals paratropic and diatropic currents for external fields pointing parallel ( $z$ -direction) and perpendicular ( $y$ -direction) to the axis of the belt, respectively (see Figure S4). When the external magnetic field points in a direction perpendicular to the belt axis (parallel to the  $y$ -axis),  $^{p\pi}\mathbf{J}^{\text{ind}}$  has a more complex topology. This change of the tropicity with respect to the orientation of the external field has also been discussed by Monaco and Zanasi using the total  $\mathbf{J}^{\text{ind}}$  calculations.<sup>68</sup> The total  $\mathbf{J}^{\text{ind}}$  shows small local current-density loops in the individual rings and a clockwise and anticlockwise rotation of the current-density flux for the upper and lower C-C bonds, respectively.  $^{p\pi}\mathbf{J}^{\text{ind}}$  suggests that the  $\pi$ -electrons create these counter-rotating currents, and, therefore, the  $\sigma$ -electrons induce the local loops shown in the total  $\mathbf{J}^{\text{ind}}$ . In the case where the external field points in the  $z$ -direction,  $^{p\pi}\mathbf{J}^{\text{ind}}$  exhibits a well-defined paratropic circulation around the carbon belt. For the latter case, the ring-current strengths from  $^{p\pi}\mathbf{J}^{\text{ind}}$  indicate that the net current is -6.57 nA/T composed of two paratropic ring-current contributions of -4.73 and -1.84 nA/T alternating in each 6-MR (see Table 2), about 20% weaker than the total one. In the case of a  $y$ -oriented external field, the global cylindrical current strength is negligible (0.01 nA/T) because there are two counter-rotating bond currents with strengths of 10.13 and -10.12 nA/T, respectively. Although the belt has a paratropic pseudo- $\pi$  current, it does not exhibit extremely strong values, even near the molecular surface, implying that there is no overestimation as in planar antiaromatic molecules.

NICS(0) computations do not provide much information about the magnetic response of this type of molecules, as Monaco and Zanasi also emphasized.<sup>68</sup> However, our analysis of  $\mathbf{B}^{\text{ind}}$  computed with an external field perpendicular to the  $z$ -direction, show the presence of a pronounced deshielding cone inside the belt due to the predominant cylindrical paratropic ring current, while the negative regions lie outside the belt (see Figure 8) in complete agreement with the current-density computations. In contrast, the  $y$ -component of  $\mathbf{B}^{\text{ind}}$  ( $B^{\text{ind}}_y$ ) is the main component of  $\mathbf{B}^{\text{ind}}$  implying that the NICS<sub>zz</sub> values are not suitable for evaluating the molecular aromaticity of [10]cyclophenacene (Figure 8). The inner region of the belt is strongly shielded because the field is directed perpendicularly to a 6-MR, resulting in a  $\mathbf{B}^{\text{ind}}$  that points in the negative  $z$ -direction.

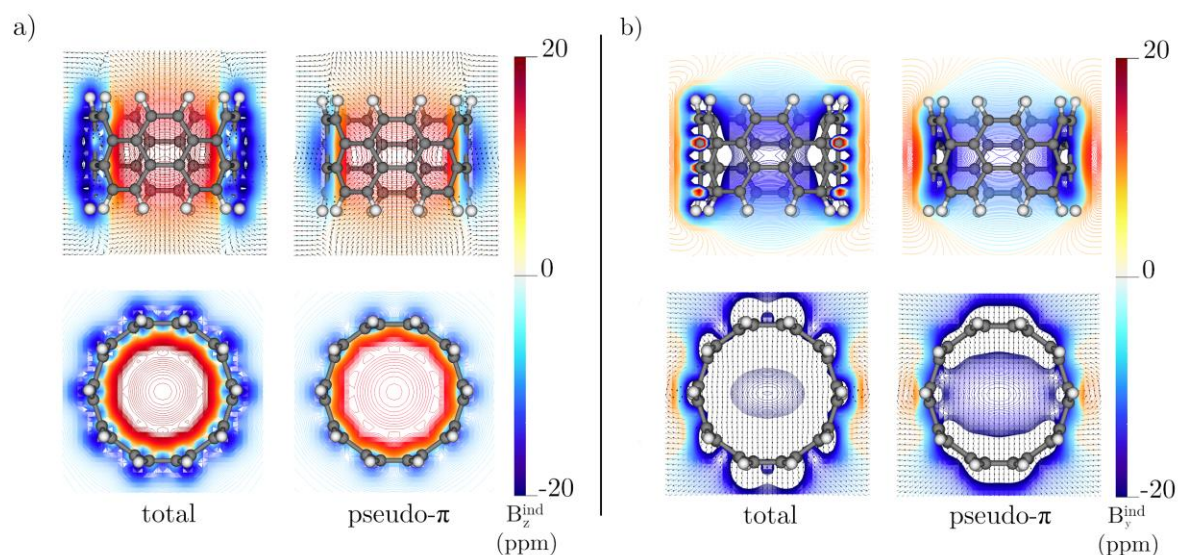


**Figure 8.** a) The total  $\mathbf{B}^{\text{ind}}$  (left) and the  ${}^{\text{p}\pi}\mathbf{B}^{\text{ind}}$  (right) calculated in the transverse plane (top) and a perpendicular plane ( $z = 0$ ) to the external field (bottom) of [10]cyclophenacene. The external field is parallel to the belt axis ( $z$ -axis). b) The total  $\mathbf{B}^{\text{ind}}$  (left) and the  ${}^{\text{p}\pi}\mathbf{B}^{\text{ind}}$  (right) calculated in the transverse plane (top) and a parallel plane ( $z = 0$ ) to the external field (bottom) of [10]cyclophenacene. The external field is parallel to the belt axis ( $y$ -axis).

### Toroidal nanotube $\text{C}_{2016}$

In the case of cylindrical CNTs, the magnetic response depends strongly on the structural parameters and the orientation of the external field with respect to the CNT.<sup>69-71</sup> When the external magnetic field is parallel to the CNT symmetry axis, the tube sustains (like [10]cyclophenacene) strong counter-rotating inner and outer ring currents.<sup>16,86</sup> When the external magnetic field is perpendicular to the CNT, the current density is diatropic inside and outside. Recently, Reiter *et al.*<sup>72</sup> calculated the magnetically induced current densities of a family of toroidal carbon nanotubes (TCNT) using the GIMIC method. When the external field is applied along the torus symmetry axis, they found that TCNTs with HOMO-LUMO gaps larger than 0.2 eV generally sustain weak global ring currents and that the ring-current strength increases with increasing TCNT size. In addition, the ring-current strengths of these large molecules depend on the functional employed, partly due to their large size.<sup>72</sup> The largest TCNTs they studied ( $\text{C}_{2016}$ ) sustains a strong ring current of about 300 nA/T (at the TPSS/def2-SVP level<sup>73</sup>). The chiral (6,3)  $\text{C}_{2016}$  TCNT also sustains a strong ring current around the tube perpendicular to the torus.<sup>72</sup> (6,3)  $\text{C}_{2016}$  is an exciting molecule for the pseudo- $\pi$  model because the all-electron  $\mathbf{J}^{\text{ind}}$  calculations in molecules of this size are computationally demanding and calculation of the  $\pi$ -component is infeasible.

The total  $\mathbf{J}^{\text{ind}}$  and  ${}^{\text{p}\pi}\mathbf{J}^{\text{ind}}$  for (6,3)  $\text{C}_{2016}$  are shown in Figure 9, where the streamline representation displays the current-density flux inside and outside the TCNT surface. The ring-current strengths were calculated at the B3LYP level and the TPSS for comparison with results obtained in previous studies.<sup>72</sup> The inner and outer  $\mathbf{J}^{\text{ind}}$  fluxes have the same tropicity, when the external magnetic field is oriented along the torus symmetry axis. The inner  $\mathbf{J}^{\text{ind}}$  flux is though somewhat weaker than that outside the surface. The total ring-current strength around the TCNT produces a global strong diatropic current of 232.3 nA/T at the TPSS level,<sup>72</sup> while B3LYP leads to 37.35 nA/T (see Table 2).  ${}^{\text{p}\pi}\mathbf{J}^{\text{ind}}$  supports that the  $\pi$ -electrons are responsible for the ring current since the ring-current strength is 416.7 nA/T and 210.43 nA/T at the TPSS and B3LYP levels, respectively. The paratropic contributions to the global current density consist mainly of local loops generated by the  $\sigma$ -electrons. The  $\mathbf{J}^{\text{ind}}$  chirality differs from that obtained with  ${}^{\text{p}\pi}\mathbf{J}^{\text{ind}}$ . In the total current-density calculation, the  $\mathbf{J}^{\text{ind}}$  pathways form a zig-zag pattern following the carbon framework. However, in  ${}^{\text{p}\pi}\mathbf{J}^{\text{ind}}$ , the pathways are more regular than those obtained in the total current-density calculation due to the absence of localized atomic current-density vortices. This implies that the vector component of the total  $\mathbf{J}^{\text{ind}}$  and  ${}^{\text{p}\pi}\mathbf{J}^{\text{ind}}$  perpendicular to the tube points in different directions, leading to different signs of the magnetically induced anapole moment (also called toroidal moment).<sup>74,75</sup> The  ${}^{\text{p}\pi}\mathbf{J}^{\text{ind}}$  flux splits at the 6-MRs and then rejoins again between the rings by coiling helically around the surface, as seen in Figure 8.

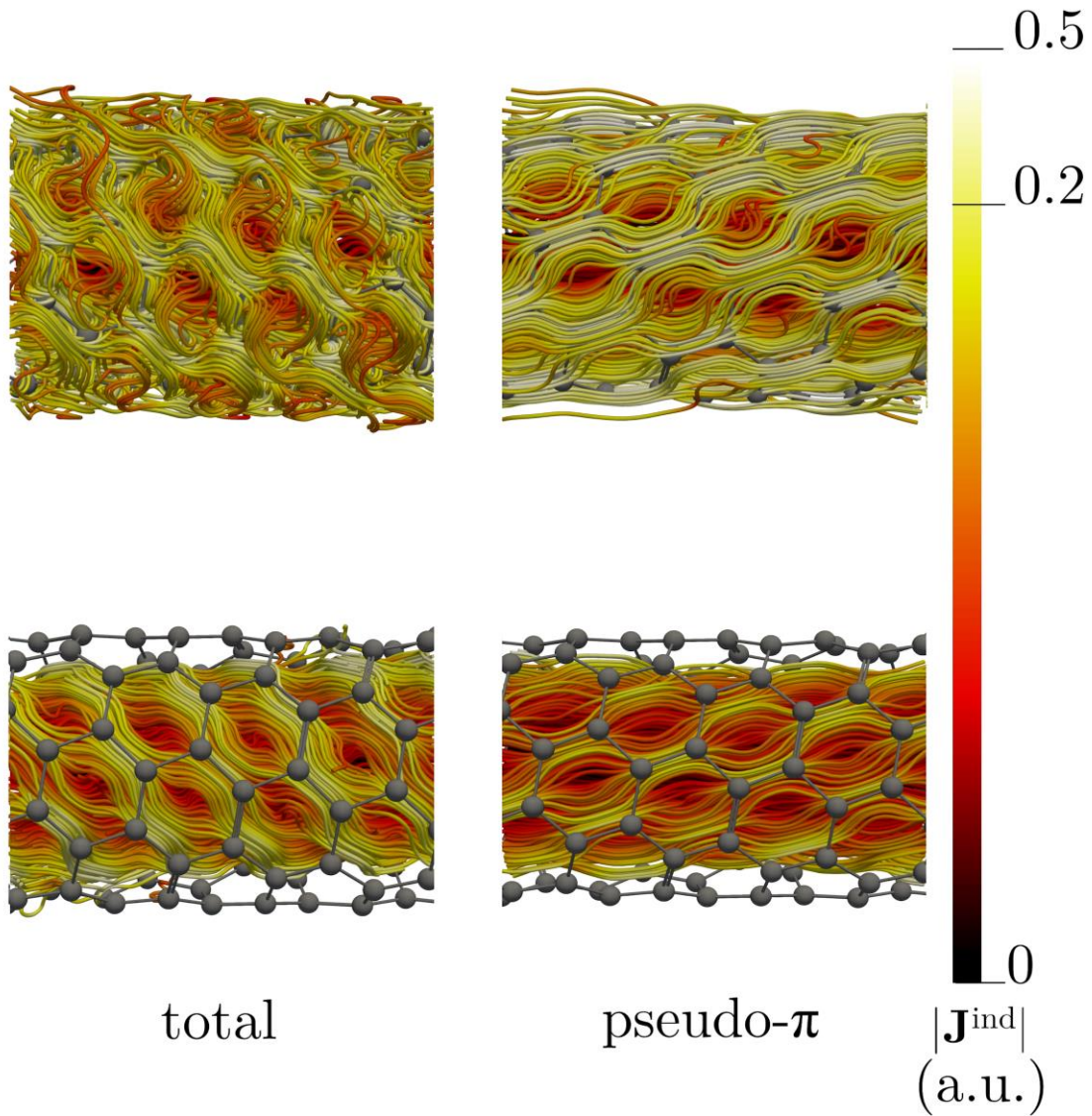


**Figure 9.** Streamlines representation of  $\mathbf{J}^{\text{ind}}$  showing the currents pathways flowing diatropically outside (top) and inside (bottom) of the surface of the toroidal carbon nanotube ( $C_{2016}$ ). The external field is parallel to the main axis of the torus.

The topology of these currents is well-known in plasma physics as *tokamaks* (helical currents around a torus surface), which can be split into poloidal and toroidal current flows, leading to a more complex magnetic behavior than that of an ideal toroidal solenoid.<sup>76-78</sup> The magnetic fields induced by such currents are susceptible to the geometric parameters of the current density giving rise to helical magnetic fields (which can also be divided into a poloidal and toroidal components) inside the torus and non-negligible magnetic fields even outside the toroidal surface.<sup>78-80</sup> Figure 10 shows that the presence of the strong  $\pi$ -current flowing on the outside and the inside the  $C_{2016}$  toroidal surface of produces a marked shielding region inside

the torus and a deshielding region on the outside of the torus. The strongest values of  ${}^{p\pi}B_z^{\text{ind}}$  are found near the edges of the toroidal surface.  ${}^{p\pi}B_x^{\text{ind}}$  and  ${}^{p\pi}B_y^{\text{ind}}$  are non-negligible inside the toroid (see Figure S5) indicating the presence of a poloidal induced magnetic field. However, these components are considerably weaker than  ${}^{p\pi}B_z^{\text{ind}}$ .  $\mathbf{B}^{\text{ind}}$  forms concentric toroidal circles around the torus surface.

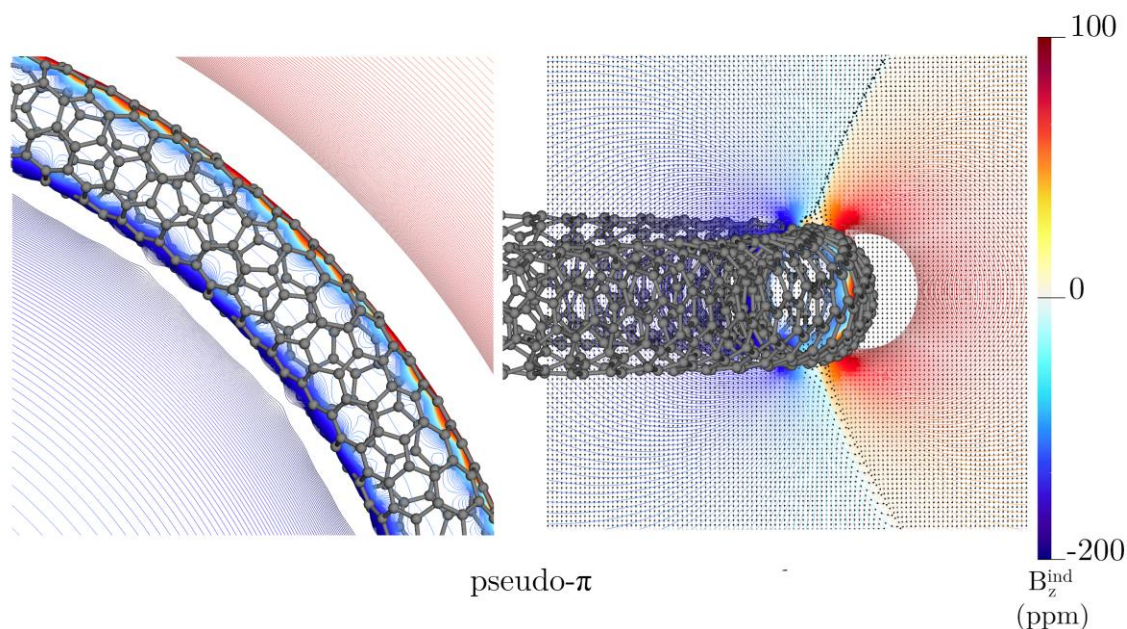


**Figure 10.**  ${}^{p\pi}\mathbf{B}$  calculated in a molecular plane (left) and a perpendicular plane (right) for  $C_{2016}$ . The arrows show the direction of  ${}^{p\pi}\mathbf{B}^{\text{ind}}$ , while the color scale denotes the strength of the  ${}^{p\pi}B_z^{\text{ind}}$ . The magnetic field is parallel to the toroidal axis.

The above discussion is more general than for  $C_{2016}$ , which is used as an example. We have also studied the magnetic response of (6,3)  $C_{2196}$ , which is another chiral TCNT. It also sustains a diatropic  ${}^{p\pi}\mathbf{J}^{\text{ind}}$  that coils helically around the toroid both inside and outside the tube, as predicted by the model (see Figure S6), leading to a ring-current strength of about 314 nA/T and 59.68 nA/T, at the TPSS and B3LYP level, respectively (see Table 2), and a similar  $B_z^{\text{ind}}$  behavior as for  $C_{2016}$  (see Figure S7). The ring-current strength of  $C_{2196}$  is only slightly weaker than for  $C_{2016}$  suggesting that the  $\pi$  ring-current strength depends mainly on the topology of the TCNT.

## Conclusions

We have used the pseudo- $\pi$  model to estimate the  $\pi$ -contribution to the magnetically induced current densities and the induced magnetic field in series of small and large planar aromatic and antiaromatic molecules as well as for non-planar molecules such as TCNTs.  ${}^{p\pi}\mathbf{J}^{\text{ind}}$  and  ${}^{p\pi}\mathbf{B}^{\text{ind}}$  agree well with data obtained in complete current-density calculations and magnetic shielding calculations dissected in their orbital contributions. We have paid particular attention to the  $\pi$ -component of the ring-current strengths because, unlike the standard total calculations, it does not suffer from the core and  $\sigma$ -electrons contamination.  ${}^{p\pi}\mathbf{J}^{\text{ind}}$  of aromatic molecules are prone to be purely diatropic.  $\mathbf{B}^{\text{ind}}$  shows that for PAHs, NICS-based indices could lead to incorrect aromatic character of the individual rings even considering the  $\pi$ -component. For example,  ${}^{p\pi}\mathbf{J}^{\text{ind}}$  support that naphthalene sustains a global ring current around the perimeter of the molecule, which it is not directly evident from  ${}^{p\pi}\mathbf{B}^{\text{ind}}$ . For coronene,  ${}^{p\pi}\mathbf{B}^{\text{ind}}$  inside the hub is negative, whereas the  ${}^{p\pi}\mathbf{J}^{\text{ind}}$  analysis shows that its local ring current is paratropic, implying that the aromatic character based on magnetic shielding needs to be carefully analyzed. Although kekulene has a diatropic ring current along the perimeter and a paratropic ring current along the inner ring, its magnetic shielding does not suffer from the same problems as coronene, since the strengths of the two ring currents are almost the same, allowing to differentiate through the  $B_z^{\text{ind}}$  values that in the center there is a paratropic and a peripheral diatropic current.

For nonplanar structures, the pseudo- $\pi$  model is quite useful, as it allows to elucidate the magnetic response at the molecular surface of large molecules without the core and  $\sigma$ -electrons contamination, which is even more pronounced in nonplanar molecules such as [10]cyclophenacene and TCNTs.  ${}^{p\pi}\mathbf{J}^{\text{ind}}$  of  $\text{C}_{60}$  is diatropic on the outside of the 6-MRs, while the paratropic ring-currents of the 5-MRs introduce distortions in global diatropic ring current.  $\text{C}_{60}$  exhibits different tropicity on the outside and the inside of the cage, which is easily perceived by plotting the  ${}^{p\pi}\mathbf{J}^{\text{ind}}$ . For the TCNTs, the total and  ${}^{p\pi}\mathbf{J}^{\text{ind}}$  have different pathways leading to different chirality of the current density flux and magnetically induced anapole moments. Thus, regardless of molecular size,  $\pi$ -electrons are the main actors in the electron delocalization in these carbon molecules. Thus, the  $\pi$ -component of the ring-current strengths for large size structures are estimated for the first time. These can be used as a direct indicator of the electron delocalization in this kind of molecular structures. Even larger systems can be studied; the molecular structures can be optimized at approximate levels of theory, whereas calculations using the pseudo- $\pi$  model involve only hydrogen atoms.

## **Acknowledgment**

The work in Mexico was supported by Conacyt (Proyecto Sinergia 1561802). This work has been supported by the Academy of Finland through project number 314821, by the Magnus Ehrnrooth Foundation, and by the Swedish Cultural Foundation in Finland. We acknowledge computational resources from the Finnish Grid and Cloud Infrastructure (persistent identifier [urn:nbn:fi:research-infras-2016072533](https://nbn-resolving.org/urn:nbn:fi:research-infras-2016072533)) and CSC- IT Center for Science, Finland. M.O.-I. and J.B. also thank CONACYT for their PhD fellowships.

## References

- (1) Ramsey, N. F. Magnetic Shielding of Nuclei in Molecules. *Phys. Rev.* **1950**, *78*, 699–703.
- (2) People, J. A. *Mol. Phys.* Proton Magnetic Resonance of Hydrocarbons. **1958**, *1*, 175–180.
- (3) McWeeny, R. Ring Currents and Proton Magnetic Resonance in Aromatic Molecules. *Mol. Phys.* **1958**, *1*, 311–321.
- (4) Lazzeretti, P. Ring Currents. *Prog. Nucl. Magn. Reson. Spectrosc.* **2000**, *36* (1), 1–88.
- (5) Valiev, R. R.; Fliegl, H.; Sundholm, D. Closed-Shell Paramagnetic Porphyrinoids. *Chem. Commun.* **2017**, *53* (71), 9866–9869.
- (6) Schleyer, P. von R.; Maerker, C.; Dransfeld, A.; Jiao, H.; van Eikema Hommes, N. J. R. Nucleus-Independent Chemical Shifts: A Simple and Efficient Aromaticity Probe. *J. Am. Chem. Soc.* **1996**, *118* (26), 6317–6318.
- (7) Geuenich, D.; Hess, K.; Köhler, F.; Herges, R. Anisotropy of the Induced Current Density (ACID), a General Method To Quantify and Visualize Electronic Delocalization. *Chem. Rev.* **2005**, *105* (10), 3758–3772.
- (8) Sundholm, D.; Fliegl, H.; Berger, R. J. F. Calculations of Magnetically Induced Current Densities: Theory and Applications. *WIREs Comput. Mol. Sci.* **2016**, 639–678.
- (9) Islas, R.; Heine, T.; Merino, G. The Induced Magnetic Field. *Acc. Chem. Res.* **2012**, *45* (2), 215–228.
- (10) Schleyer, P. v. R. Introduction: Aromaticity. *Chem. Rev.* **2001**, *101* (5), 1115–1118.
- (11) Merino, G.; Solà, M. Celebrating the 150th Anniversary of The Kekulé Benzene Structure. *Phys. Chem. Chem. Phys.* **2016**, *18*, 11587–11588.
- (12) Jusélius, J.; Sundholm, D.; Gauss, J. Calculation of Current Densities Using Gauge-Including Atomic Orbitals. *J. Chem. Phys.* **2004**, *121* (9), 3952–3963.
- (13) Fowler, P. W.; Steiner, E. Pseudo- $\pi$  Currents: Rapid and Accurate Visualisation of Ring Currents in Conjugated Hydrocarbons. *Chem. Phys. Lett.* **2002**, *364*, 259–266.
- (14) Charistos, N. D.; Muñoz-Castro, A.; Sigalas, M. P. The Pseudo- $\pi$  Model of the Induced Magnetic Field: Fast and Accurate Visualization of Shielding and Deshielding Cones in Planar Conjugated Hydrocarbons and Spherical Fullerenes. *Phys. Chem. Chem. Phys.* **2019**, *21*, 6150–6159.
- (15) Becke, A. D. Density-functional Thermochemistry. III. The Role of Exact Exchange. *J. Chem. Phys.* **1993**, *98*, 5648–5652.
- (16) Wirz, L. N.; Dimitrova, M.; Fliegl, H.; Sundholm, D. Magnetically Induced Ring-Current Strengths in Möbius Twisted Annulenes. *J. Phys. Chem. Lett.* **2018**, *9* (7), 1627–1632.
- (17) Valiev, R. R.; Benkyi, I.; Konyshv, Y. V.; Fliegl, H.; Sundholm, D. Computational Studies of Aromatic and Photophysical Properties of Expanded Porphyrins. *J. Phys. Chem. A.* **2018**, *122* (20), 4756–4767.
- (18) Lehtola, S.; Dimitrova, M.; Fliegl, H.; Sundholm, D. Benchmarking Magnetizabilities with Recent Density Functionals. *J. Chem. Theory Comput.* **2021**, *17* (3), 1457–1468.
- (19) Grimme, S.; Antony, J.; Ehrlich, S.; Krieg, H. A Consistent and Accurate Ab Initio Parametrization of Density Functional Dispersion Correction (DFT-D) for the 94 Elements H-Pu. *J. Chem. Phys.* **2010**, *132* (15), 154104.
- (20) Weigend, F.; Ahlrichs, R. Balanced Basis Sets of Split Valence, Triple Zeta Valence

- and Quadruple Zeta Valence Quality for H to Rn: Design and Assessment of Accuracy. *Phys. Chem. Chem. Phys.* **2005**, *7* (18), 3297–3305.
- (21) Ditchfield, R. Self-Consistent Perturbation Theory of Diamagnetism. *Mol. Phys.* **1974**, *27* (4), 789–807.
  - (22) Wolinski, K.; Hinton, J. F.; Pulay, P. Efficient Implementation of the Gauge-Independent Atomic Orbital Method for NMR Chemical Shift Calculations. *J. Am. Chem. Soc.* **1990**, *112* (23), 8251–8260.
  - (23) Ahlrichs, R.; Bär, M.; Häser, M.; Horn, H.; Kölmel, C. Electronic Structure Calculations on Workstation Computers: The Program System Turbomole. *Chem. Phys. Lett.* **1989**, *162* (3), 165–169.
  - (24) Furche, F.; Ahlrichs, R.; Hättig, C.; Klopper, W.; Sierka, M.; Weigend, F. Turbomole. *WIREs Comput. Mol. Sci.* **2014**, *4*, 91–100.
  - (25) Fliegl, H.; Taubert, S.; Lehtonen, O.; Sundholm, D. The Gauge Including Magnetically Induced Current Method. *Phys. Chem. Chem. Phys.* **2011**, *13* (46), 20500–20518.
  - (26) Merino, G.; Heine, T.; Seifert, G. The Induced Magnetic Field in Cyclic Molecules. *Chem. – Eur. J.* **2004**, *10*, 4367–4371.
  - (27) Heine, T.; Islas, R.; Merino, G.  $\sigma$  and  $\pi$  Contributions to the Induced Magnetic Field: Indicators for the Mobility of Electrons in Molecules. *J. Comput. Chem.* **2007**, *28*, 302–309.
  - (28) Orozco-Ic, M.; Cabellos, J. L.; Merino, G. *Aromagnetic*. **2016**, Cinvestav-Merida.
  - (29) Anet, F. A. L.; O’Leary, D. J. The Shielding Tensor. Part I: Understanding Its Symmetry Properties. *Concepts Magn. Reson. Part A*. **1991**, *3*, 193–214.
  - (30) Fallah-Bagher-Shaidaei, H.; Wannere, C. S.; Corminboeuf, C.; Puchta, R.; Schleyer, P. v. R. Which NICS Aromaticity Index for Planar Pi Rings Is Best? *Org. Lett.* **2006**, *8* (5), 863–866.
  - (31) Ahrens, J.; Geveci, B.; Law, C. ParaView: An End-User Tool for Large-Data Visualization. *Visualization Handbook*. **2005**, 717–731.
  - (32) Wes Bethel, E.; Childs, H.; Hansen, C. *High Performance Visualization: Enabling Extreme-Scale Scientific Insight*; CRC Press, **2012**.
  - (33) Monaco, G.; Zanasi, R. Assessment of Ring Current Models for Monocycles. *J. Phys. Chem. A*. **2014**, *118* (9), 1673–1683.
  - (34) Monaco, G.; Zanasi, R.; Pelloni, S.; Lazzarotti, P. Relative Weights of  $\sigma$  and  $\pi$  Ring Currents in a Few Simple Monocycles. *J. Chem. Theory Comput.* **2010**, *6* (11), 3343–3351.
  - (35) Berger, R. J. F.; Viel, A. The Symmetry Principle of Antiaromaticity. *Z. Naturforsch. B*. **2020**, *75* (4), 327–339.
  - (36) Szczepanik, D. W.; Solà, M.; Andrzejak, M.; Pawełek, B.; Dominikowska, J.; Kukułka, M.; Dyduch, K.; Krygowski, T. M.; Szatyłowicz, H. The Role of the Long-Range Exchange Corrections in the Description of Electron Delocalization in Aromatic Species. *J. Comput. Chem.* **2017**, *38* (18), 1640–1654.
  - (37) Torrent-Sucarrat, M.; Navarro, S.; Cossío, F. P.; Anglada, J. M.; Luis, J. M. Relevance of the DFT Method to Study Expanded Porphyrins with Different Topologies. *J. Comput. Chem.* **2017**, *38* (32), 2819–2828.
  - (38) Casademont-Reig, I.; Woller, T.; Contreras-García, J.; Alonso, M.; Torrent-Sucarrat, M.; Matito, E. New Electron Delocalization Tools to Describe the Aromaticity in Porphyrinoids. *Phys. Chem. Chem. Phys.* **2018**, *20* (4), 2787–2796.
  - (39) Steiner, E.; Fowler, P. W.; Havenith, R. W. A. Current Densities of Localized and Delocalized Electrons in Molecules. *J. Phys. Chem. A*. **2002**, *106* (30), 7048–7056.
  - (40) Steiner, E.; Fowler, P. W. Patterns of Ring Currents in Conjugated Molecules: A

- Few-Electron Model Based on Orbital Contributions. *J. Phys. Chem. A* **2001**, *105* (41), 9553–9562.
- (41) Steiner, E.; Fowler, P. W.; Jenneskens, L. W. Counter-Rotating Ring Currents in Coronene and Corannulene. *Angew. Chem., Int. Ed.* **2001**, *40*(2), 362–366.
- (42) Aihara, J.-I. The Origin of Counter-Rotating Rim and Hub Currents in Coronene. *Chem. Phys. Lett.* **2004**, *393*, 7–11.
- (43) Monaco, G.; Viglione, R. G.; Zanasi, R.; Fowler, P. W. Designing Ring-Current Patterns: [10,5]-Coronene, a Circulene with Inverted Rim and Hub Currents. *J. Phys. Chem. A* **2006**, *110* (23), 7447–7452.
- (44) Aihara, J.-I. A Simple Method for Estimating the Superaromatic Stabilization Energy of a Super-Ring Molecule. *J. Phys. Chem. A* **2008**, *112* (18), 4382–4385.
- (45) Haags, A.; Reichmann, A.; Fan, Q.; Egger, L.; Kirschner, H.; Naumann, T.; Werner, S.; Vollgraff, T.; Sundermeyer, J.; Eschmann, L.; Yang, X.; Brandstetter, D.; Bocquet, F. C.; Koller, G.; Gottwald, A.; Richter, M.; Ramsey, M. G.; Rohlfing, M.; Puschnig, P.; Gottfried, J. M.; Soubatch, S.; Tautz, F. S. Kekulene: On-Surface Synthesis, Orbital Structure, and Aromatic Stabilization. *ACS Nano* **2020**, *14* (11), 15766–15775.
- (46) Steiner, E.; Fowler, P. W.; Acocella, A.; Jenneskens, L. W. Visualisation of Counter-Rotating Ring Currents in Kekulene. *Chem. Comm.* **2001**, *7*, 659–660.
- (47) Chen, Z.; Wu, J. I.; Corminboeuf, C.; Bohmann, J.; Lu, X.; Hirsch, A.; Schleyer, P. von R. Is C<sub>60</sub> Buckminsterfullerene Aromatic? *Phys. Chem. Chem. Phys.* **2012**, *14* (43), 14886–14891.
- (48) Zanasi, R.; Fowler, P. W. Ring Currents and Magnetisability in C<sub>60</sub>. *Chem. Phys. Lett.* **1995**, *238*, 270–280.
- (49) Johansson, M. P.; Jusélius, J.; Sundholm, D. Sphere Currents of Buckminsterfullerene. *Angew. Chem., Int. Ed.* **2005**, *44*, 1877–1880.
- (50) Charistos, N. D.; Muñoz-Castro, A. Induced Magnetic Field of Fullerenes: Role of  $\sigma$ - and  $\pi$ - Contributions to Spherical Aromatic, Nonaromatic, and Antiaromatic Character in C<sub>60</sub><sup>q</sup> (q = 10, 0, -6, -12), and Related Alkali-Metal Decorated Building Blocks, Li<sub>12</sub>C<sub>60</sub> and Na<sub>6</sub>C<sub>60</sub>. *J. Phys. Chem. C* **2018**, *122* (17), 9688–9698.
- (51) Sundholm, D.; Wirz, L. N.; Schwerdtfeger, P. Novel Hollow All-Carbon Structures. *Nanoscale* **2015**, *7* (38), 15886–15894.
- (52) Sundholm, D. C<sub>72</sub>: Gaudiene, a Hollow and Aromatic All-Carbon Molecule. *Phys. Chem. Chem. Phys.* **2013**, *15* (23), 9025–9028.
- (53) Schwerdtfeger, P.; Wirz, L. N.; Avery, J. The Topology of Fullerenes. *WIREs Comput. Mol. Sci.* **2015**, *5* (1), 96–145.
- (54) Hirsch, A.; Chen, Z.; Jiao, H. Spherical Aromaticity in Symmetrical Fullerenes: The 2(N+1) Rule. *Angew. Chem., Int. Ed.* **2000**, *39* (21), 3915–3917.
- (55) Rauhalhti, M.; Muñoz-Castro, A.; Sundholm, D. Magnetic Response Properties of Gaudiene – a Cavernous and Aromatic Carbocage. *Phys. Chem. Chem. Phys.* **2016**, *18*, 18880–18886.
- (56) Orozco-Ic, M.; Barroso, J.; Charistos, N. D.; Muñoz-Castro, A.; Merino, G. Consequences of the Curvature on the Induced Magnetic Field: Case of Helicenes. *Chem. – Eur. J.* **2020**, *26*, 326–330.
- (57) Cherni, E.; Champagne, B.; Ayadi, S.; Liégeois, V. Magnetically-Induced Current Density Investigation in Carbohelicenes and Azahelicenes. *Phys. Chem. Chem. Phys.* **2019**, *21* (27), 14678–14691.
- (58) Portella, G.; Poater, J.; Bofill, J. M.; Alemany, P.; Solà, M. Local Aromaticity of [n]Acenes, [n]Phenacenes, and [n]Helicenes (n= 1–9). *J. Org. Chem.* **2005**, *70* (7), 2509–2521.

- (59) Kalam, H.; Kerim, A.; Najmidin, K.; Abdurishit, P.; Tawar, T. A Study on the Aromaticity of [n]phenacenes and [n]helicenes (n= 3–9). *Chem. Phys. Lett.* **2014**, *592*, 320–325.
- (60) Schulman, J. M.; Disch, R. L. Aromatic Character of [n]Helicenes and [n]Phenacenes. *J. Phys. Chem. A.* **1999**, *103* (33), 6669–6672.
- (61) Evans, P. J.; Jasti, R. Molecular Belts. *Top. Curr. Chem.* **2014**, *349*, 249–290.
- (62) Segawa, Y.; Yagi, A.; Ito, H.; Itami, K. A Theoretical Study on the Strain Energy of Carbon Nanobelts. *Org. Lett.* **2016**, *18* (6), 1430–1433.
- (63) Nakamura, E.; Tahara, K.; Matsuo, Y.; Sawamura, M. Synthesis, Structure, and Aromaticity of a Hoop-Shaped Cyclic Benzenoid [10]cyclophenacene. *J. Am. Chem. Soc.* **2003**, *125* (10), 2834–2835.
- (64) Yao, T.; Yu, H.; Vermeij, R. J.; Bodwell, G. J. Nonplanar Aromatic Compounds. Part 10: A Strategy for the Synthesis of Aromatic Belts-All Wrapped up or down the Tubes? *Pure App. Chem.* **2008**, 533–546.
- (65) Wegner, H. A. On the Way to Carbon Nanotubes: The First Synthesis of an Aromatic Nanobelt. *Angew. Chem. Int. Ed Engl.* **2017**, *56* (37), 10995–10996.
- (66) Tian, X.; Jasti, R. Cycloparaphenylenes: The Shortest Possible Segments of Armchair Carbon Nanotubes. *Fragments of Fullerenes and Carbon Nanotubes.* **2011**, 291–309.
- (67) Muñoz-Castro, A. Local and Global Aromaticity in a Molecular Carbon Nanobelt: Insights from Magnetic Response Properties in Neutral and Charged Species. *Phys. Chem. Chem. Phys.* **2018**, *20*, 3433–3437.
- (68) Monaco, G.; Zanasi, R. Analysis of the Nucleus-Independent Chemical Shifts of [10]Cyclophenacene: Is It an Aromatic or Antiaromatic Molecule? *J. Phys. Chem. Lett.* **2017**, *8* (19), 4673–4678.
- (69) Kibalchenko, M.; Payne, M. C.; Yates, J. R. Magnetic Response of Single-Walled Carbon Nanotubes Induced by an External Magnetic Field. *ACS Nano.* **2011**, *5* (1), 537–545.
- (70) Linert, W.; Lukovits, I. Aromaticity of Carbon Nanotubes. *J. Chem. Inf. Model.* **2007**, *47* (3), 887–890.
- (71) Ren, P.; Zheng, A.; Xiao, J.; Pan, X.; Bao, X. Exploring the Ring Current of Carbon Nanotubes by First-Principles Calculations. *Chem. Sci.* **2015**, *6* (2), 902–908.
- (72) Reiter, K.; Weigend, F.; Wirz, L. N.; Dimitrova, M.; Sundholm, D. Magnetically Induced Current Densities in Toroidal Carbon Nanotubes. *J. Phys. Chem. C.* **2019**, *123*, 15354–15365.
- (73) Tao, J.; Perdew, J. P.; Staroverov, V. N.; Scuseria, G. E. Climbing the Density Functional Ladder: Nonempirical Meta-Generalized Gradient Approximation Designed for Molecules and Solids. *Phys. Rev. Lett.* **2003**, *91* (14), 146401.
- (74) Ceulemans, A.; Chibotaru, L. F.; Fowler, P. W. Molecular Anapole Moments. *Phys. Rev. Lett.* **1998**, *80*, 1861–1864.
- (75) Pelloni, S.; Lazzarotti, P.; Monaco, G.; Zanasi, R. Magnetic-Field Induced Electronic Anapoles in Small Molecules. *Rend. Lincei.* **2011**, *22*, 105–112.
- (76) Dubovik, V. M.; Tugushev, V. V. Toroid Moments in Electrodynamics and Solid-State Physics. *Phys. Rep.* **1990**, *187* (4), 145–202.
- (77) Bhadra, D. Field Due to Current in Toroidal Geometry. *Rev. Sci. Instr.* **1968**, *39*, 1536–1546.
- (78) Pahlavani, M. R. A.; Shoulaie, A. A Novel Approach for Calculations of Helical Toroidal Coil Inductance Usable in Reactor Plasmas. *IEEE Trans. Plasma Sci.* **2009**, *37* (8), 1593–1603.
- (79) Martín, P.; Haines, M. G. Poloidal Magnetic Field around a Tokamak Magnetic

- Surface. *Phys. Plasmas*. **1998**, 5 (2), 410–416.
- (80) Kucinski, M. Y.; Caldas, I. L. Toroidal Helical Fields. *Z. Naturforsch. A*. **1987**, 42, 1124–1132.